INDONESIAN JOURNAL ON GEOSCIENCE
Geological Agency
Ministry of Energy and Mineral Resources

Journal homepage: https://ijog.geologi.esdm.go.id
ISSN 2355-9314, e-ISSN 2355-9306

Subsurface Modeling Using Gravity Data in Southern Yogyakarta and Its Implications for The May 26th, 2006 Earthquake

Muhammad Irham Nurwidyanto[1], Tony Yulianto[1], Rina Dwi Indriana[1], and Adelia Nanda Pramudya[2]

[1]Department of Physics, Faculty of Science and Mathematics, Diponegoro University, Semarang, Indonesia
[2]Master's Program in Physics, Faculty of Science and Mathematics, Diponegoro University, Semarang, Indonesia

Corresponding author: irhammn@lecturer.undip.ac.id
Manuscript received: September 21, 2025; revised: November 19, 2025;
approved: April 27, 2026; available online: October 21, 2026

Abstract - The Yogyakarta region is one of the most seismically vulnerable areas in Indonesia, so detailed subsurface fault characterization is crucial for effective disaster mitigation strategies. Previous studies have recognized the Opak Fault as the main structure controlling seismicity in this area, but the geometry and existence of other fault systems remain less constrained. This study aims to delineate the subsurface density variations associated with fault zones and rock deformation. This study develops a two-dimensional gravity inversion model to refine the subsurface configuration of faults in southern Yogyakarta. Gravity data were processed through standard corrections and anomaly separation to generate a complete Bouguer anomaly and residual anomalies. The results show that residual anomalies (-60 to 100 mgal) successfully delineate lithological variations, where older volcanic units (Semilir, Nglanggeran, and Sambipitu Formations) produce positive density contrasts (0.4-0.85 g/cm³), while younger Merapi deposits display negative contrasts (-0.5 to -0.05 g/cm³). Importantly, the 2D model highlights not only the Opak Fault but also the Ngalang Fault to the east, spatially coinciding with the 26th May 2006 earthquake epicentre. This finding provides new evidence of the structural complexity in southern Yogyakarta and emphasizes the role of the Ngalang Fault in regional seismicity, offering an updated basis for seismic hazard assessment in the area.
Keywords: Opak Fault, Ngalang Fault, seismic hazard, disaster mitigation, Bouguer anomaly, density contrast

© IJOG - 2026

How to cite this article:
Nurwidyanto, M.I., Yulianto, T., Indriana, R.D., and Pramudya, A.N., 2026. Subsurface Modeling Using Gravity Data in Southern Yogyakarta and Its Implications for The May 26th, 2006 Earthquake. *Indonesian Journal on Geoscience*, 13 (3), p.487-501. DOI:-0.17014/ ijog.13.3.487-501

Introduction

Background

The Yogyakarta earthquake occurred on May 26th, 2006, at 22:53:58 UTC with a magnitude of ~6.4, causing severe infrastructure damage, numerous casualties, and significant economic losses (Perdana and Castello, 2025). This earthquake was initially attributed to the Opak Fault, as the most severe damage was concentrated in Bantul District, located near this fault system. However, several previous studies, including those conducted by the German Task Force for Earthquake (GTF), reported that most aftershocks following the May 26th event were located more than 10 km east of the Opak Fault (Walter, 2006; Hasanudin *et al*., 2009; Handayani, 2019; Fitrianingtyas *et al*., 2023). Furthermore, Interferometric Synthetic Aperture Radar (InSAR) analysis indicated that no surface deformation was detected along the Opak Fault zone (Tsuji *et al*., 2009). Consequently, a number of studies utilizing seismic tomography,

PUBLISHED IN IJOG

hypocentre relocation, and stress analysis suggested that the mainshock did not occur on the Opak Fault but rather on an unidentified fault located further east.

One of the important studies of the 2006 Yogyakarta earthquake conducted by Diambama *et al*. (2019) revealed the velocity structure within the earthquake zone. Using Vp/Vs ratio tomography inversion from aftershock data near the Opak Fault, the study demonstrated that most aftershocks were distributed 10-15 km east of the Opak Fault. In addition, velocity anomalies down to depths of 5-7 km were identified, indicating the presence of a through-going fault with strike-slip and reverse components dipping eastward. Subsequently, Librian (2024) performed seismic tomography with finer grid spacing to model both the Opak Fault and an eastern structure identified as the Ngalang Fault. The study suggested an additional structural contribution from the Oyo Fault, which connects the Opak Fault with eastern fault segments. Ramdhan *et al.* (2025) further analyzed the seismicity using a 1D velocity model and relocated 2,141 hypocentres out of 2,170 recorded earthquakes. The results revealed the presence of aftershocks along the southern segment of both the Opak Fault and the Oyo Fault, supported by the distribution of high static stress.

Previous studies have provided an overview of the velocity structure responsible for the 2006 Yogyakarta earthquake. However, these investigations mainly describe the elastic properties of the rocks while neglecting subsurface density variations, which play a key role in fault dynamics. The present research complements these studies by applying the gravity method to investigate previously unaddressed parameters. Gravity analysis is particularly relevant in this context, as it allows the delineation of subsurface density variations that correspond to fault zones and rock damage through contrasts in lithology across fault boundaries. By utilizing gravity data, anomalous rock bodies can be mapped based on density contrasts, providing a more comprehensive interpretation of fault positions and characteristics.

Based on this background, the objective of this study is to identify the fault responsible for the 2006 Yogyakarta earthquake. Although previous research has provided insights into the likely source fault, information on rock density parameters, which are essential for characterizing weak zones, remains limited. Therefore, this study processes gravity data through Bouguer and terrain corrections to obtain representative gravity anomalies. These anomalies are subsequently analyzed to determine earthquake source depths through regional-residual anomaly separation and Euler deconvolution. Furthermore, a two-dimensional inversion was carried out to model the subsurface density distribution, thereby complementing seismic tomography studies and providing a more comprehensive understanding of the subsurface structure in the studied area.

Geological and Stratigraphical Framework

The southern part of Yogyakarta is characterized by diverse lithostratigraphy resulting from a long history of sedimentary processes. Several geological formations are found within the studied area, each formed through different depositional environments. The Semilir and Nglanggeran Formations were deposited during the Late Eocene to Early Miocene. The Semilir Formation is dominated by tuff, sandstone, and breccia, while the Nglanggeran Formation mainly consists of volcanic breccia intercalated with andesitic lava. During the subsequent period, from the Middle Miocene to Late Miocene, the Sambipitu, Wonosari, Kepek, and Sentolo Formations were developed. The Sambipitu Formation is characterized by clastic sediments and volcanic breccia, whereas the Wonosari Formation is dominated by limestone. Overlying the Wonosari Formation is the Kepek Formation, composed of marl with intercalations of limestone, while to the west lies the Sentolo Formation, consisting of claystone, sandstone, and marl. Finally, during the Quaternary period, deposits of the Merapi volcanic rocks were formed. Figure 1 shows the geological map of the studied area.

PUBLISHED IN IJOG

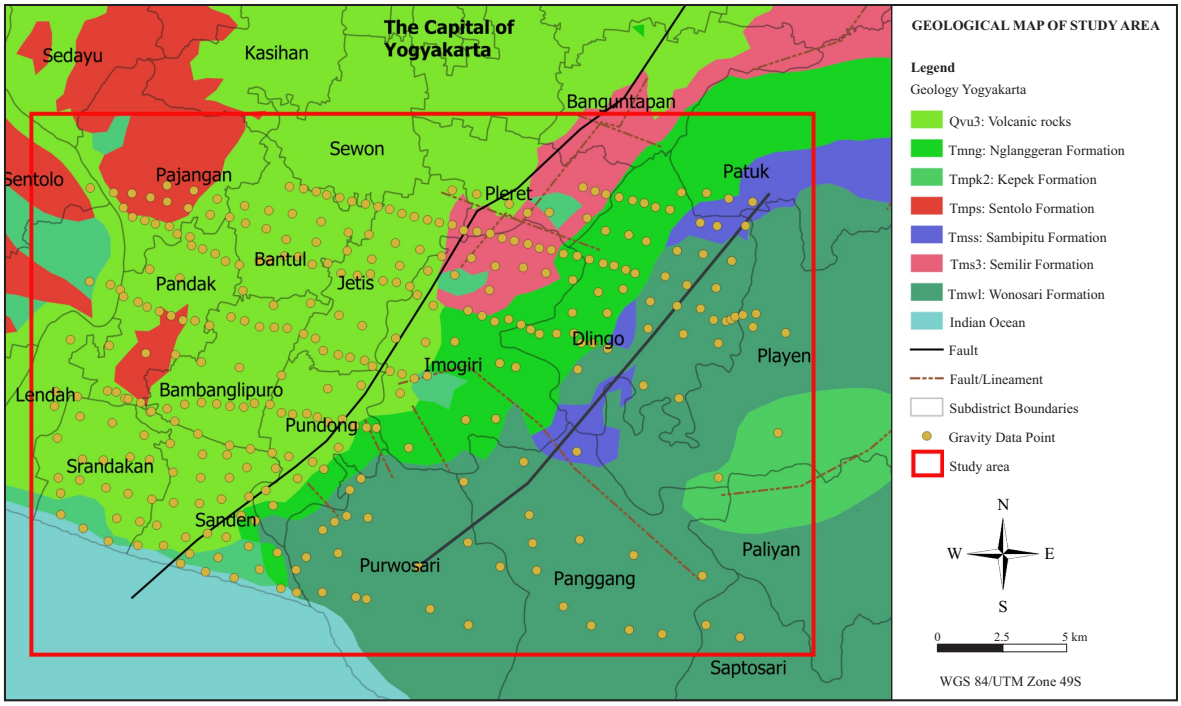


Figure 1. Geological map of the studied area (modified from Indonesia Geospatial Shapefile Map) The dashed lines indicate the presence of faults; the bold solid lines represent identified faults, the yellow circles represent the gravity data acquisition points, and the grey solid lines denote subdistrict boundaries.

The severe damage caused by the 2006 Yogyakarta earthquake was closely related to the area's subsurface geological conditions. The studied area is generally covered by alluvial deposits and young volcanic rocks that are unconsolidated and poorly compacted, resulting in low seismic attenuation capacity and significant amplification of seismic waves (Moon *et al*., 2017; Famiani *et al*., 2020; Panzera *et al*., 2020). The eastern region comprises the Nglanggeran, Semilir, Sambipitu, and Kepek Formations, which exhibit extensive fracturing due to past tectonic activity (Mulyaningsih, 2021; Surono, 2008; Rizkianto, 2022). The Wonosari Formation also shows evidence of repeated volcanic activity since the Oligo-Miocene period, which subsequently formed gentle folds and uplifted structures (Pohan *et al*., 2023). This diverse lithological composition, combined with the presence of the north-south-trending Opak Fault that cuts across unconsolidated sedimentary zones, produces a heterogeneous response to seismic wave propagation. Sedimentary zones tend to amplify ground motion, whereas active fault zones act as pathways for the release of earthquake energy.

Methods and Materials

Methods

The gravity method is one of the geophysical exploration techniques used to calculate variations in the Earth's gravitational field. These variations are caused by differences in the density of subsurface rocks. The fundamental theory of the gravity method is Newton's Law, which states that the force between two objects is proportional to the product of their masses and inversely proportional to the square of the distance between them. The gravity data obtained from field measurements were then processed through a series of data processing and interpretation stages, as illustrated in Figure 2.

Gravity data processing begins with corrections for instrumental drift and tidal effects. Drift values are obtained from the difference in repeated measurements at the base station relative to the observation stations. Tidal corrections are performed based on the acquisition time and the position of the observation points. Latitude corrections were then applied using GPS measure-

PUBLISHED IN IJOG

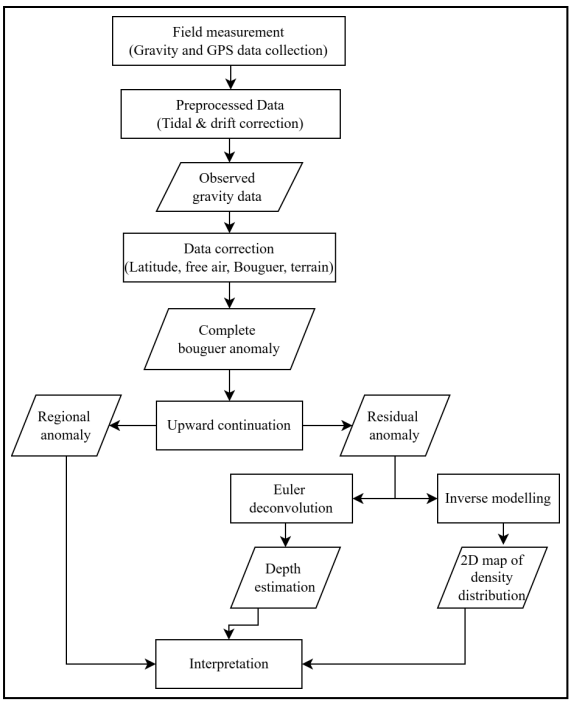


Figure 2. Data processing workflow showing the steps of data processing This process involves data collection and interpretation to develop the subsurface structural and depth model.

ments collected in the field, which were subsequently used to calculate the correction values at each observation point. The acquired gravity data were further corrected for free-air, Bouguer, and terrain effects. The resulting Complete Bouguer Anomaly is expressed in Equation (1).

$$CBA = g_{obs} + FAC - BC - TC \quad \text{..... (1)}$$

where:
g_{obs} is the gravity value obtained during field acquisition,
FAC is the free-air correction,
BC is the Bouguer correction, and
TC is the terrain correction.

The Complete Bouguer Anomaly (CBA) represents a superposition of data from various depths; therefore, anomaly separation is required to distinguish residual anomalies (shallow sources) from regional anomalies (deeper sources). The separation was performed using the upward continuation method, which was mathematically expressed in Equation (2) (Blakely, 1996).

$$(x, y, z_0 - \Delta z) = \frac{\Delta z}{2\pi} \int_{-\infty}^{\infty} \frac{U(x', y', z_0')}{\left[(x-x')^2 - (y-y') + \Delta z^2\right]^{3/2}} \quad \text{..... (2)}$$

where $\Delta z>0$.

Subsequently, the depth of the anomalies was mapped using the Euler deconvolution method. Initially, this method was widely applied to estimate the depth of hydrocarbon reservoirs; however, over time it has also been utilized to estimate the depth of gravity anomalies. The Euler deconvolution can be mathematically expressed in Equation (3) (Blakely, 1996).

$$\left[\frac{\partial}{\partial x} g_i \frac{\partial}{\partial y} g_i \frac{\partial}{\partial z} g_i\right] \begin{bmatrix} x - x_0 \\ y - y_0 \\ z - z_0 \end{bmatrix} = n.g_i \quad \text{..... (3)}$$

g_i is the gravity anomaly value,

$\frac{\partial}{\partial x} g_i \frac{\partial}{\partial y} g_i \frac{\partial}{\partial z} g_i$ are the spatial derivatives of the gravity anomaly,
$x_0 y_0 z_0$ are the coordinates of the anomaly source,
n is the structural index representing the source geometry.

To further model the subsurface density distribution, gravity inversion was performed. The inverse modeling is expressed in a matrix form as Equation (4).

$$d = G_m + e \quad \text{..... (4)}$$

where:
d is the vector of observed gravity anomalies,
G is the sensitivity matrix relating model parameters to observation.
m is the vector of subsurface density parameters,
e represents measurement errors.

This gravity technique is used to examine regional-scale basins and geological formations. Advances in gravity assessment using full tensor gravity (FTG) can support both basin evaluation and geological formation mapping (Mahendra *et al*., 2026). This study concentrates on analysing gravity anomalies according to their intensity, form, and spatial arrangement to elucidate geo-

PUBLISHED IN IJOG

logical formations and lithology in the southern Yogyakarta area and to investigate their relevance to the earthquake of 26 May 2006. Furthermore, the depth estimated from Euler deconvolution is interpreted in relation to known geological structures and lithologies. For instance, shallow sources inferred from residual anomalies may represent volcanic or alluvial deposits, while deeper regional anomalies may correspond to basement highs or structural troughs. The result of the inverse modeling provides a two-dimensional distribution of subsurface density. High-density zones revealed by the inversion are interpreted as intrusive igneous bodies, while low-density zones correspond to sedimentary layers, alluvial deposits, or potential cavities. The spatial extent, depth, and contrast of the density anomalies are analyzed to identify geological structures such as faults. Areas with sharp density contrast may indicate fault zones. Therefore, the distribution of high- and low-density anomalies can help identify potential earthquake-prone areas and active fault systems.

Materials

This study utilized gravity data obtained from field measurements conducted in the southern part of Yogyakarta (Bantul and Wonosari Regencies), within the coordinates of 417,253 m E - 445,778 m E and 9,111,360 m N - 9,128,998 m N. A total of 327 measurement stations were established across the studied area, as illustrated in Figure 1 by the small yellow circles. The field survey was carried out from 11th to 23rd August 2010. Measurements were carried out using a La-Coste & Romberg gravimeter, type G-1118 MVR, with an accuracy on the order of μgal (1 gal = 1 cm/s²). The position of each measurement point was recorded using a Trimble Navigation GPS, type 4600 LS, along with a Garmin GPS III Plus unit for field orientation. Additional equipment included a geological compass, geological maps, topographic maps, and field notebooks. The geographic coordinate system was employed during data acquisition, which was subsequently converted into UTM Zone 49S (WGS84) during data processing.

Result and Analysis

Data Correction Result

Prior to obtaining the observed gravity, the raw gravity meter readings were corrected through several preprocessing steps. These included tidal correction, which removes the influence of lunar and solar gravitational forces, and instrument drift correction, which accounts for changes in normal gravity with latitude. After applying these corrections, the adjusted gravity values were used to compute Δg, from which the final observed gravity was obtained (Table 1). The resulting observed gravity map (Figure 3) represents the gravity field after tidal and drift corrections. At this stage, the spatial pattern is still strongly controlled by topography, with lower gravity values occurring in high-elevation regions and higher values concentrated in lowlands.

Table 1. An excerpt of the gravity correction table, including tidal and drift corrections used to obtain the observed gravity (g obs) for stations 131- 144. The full dataset consists of 327 stations.

Station	Latitude	Elevation	Gravimeter reading	Tide corr	Δg tide	Drift corr	Δg drift	G obs
131	7.866661	85.41	1836.49	0.03	1836.56	-0.12	1836.68	978215.87
132	7.867769	84.23	1837.44	0.00	1837.57	-0.11	1837.67	978216.86
133	7.868878	82.76	1838.98	-0.02	1839.08	-0.10	1839.18	978218.37
134	7.870002	81.94	1840.67	-0.02	1840.82	-0.10	1840.92	978220.11
136	7.873066	79.92	1846.19	0.09	1846.14	-0.02	1846.16	978225.35
137	7.873375	83.81	1845.30	0.08	1845.29	-0.02	1845.31	978224.50
138	7.874133	84.55	1845.09	0.06	1845.17	-0.03	1845.20	978224.39
139	7.875430	85.67	1845.07	0.05	1845.13	-0.04	1845.17	978224.36
141	7.877703	133.87	1832.29	0.03	1832.39	-0.05	1832.44	978211.63
142	7.878653	92.95	1840.97	0.01	1841.06	-0.06	1841.11	978220.30
143	7.879745	93.47	1839.70	-0.01	1839.99	-0.07	1840.06	978219.25
144	7.881129	125.01	1832.81	-0.01	1832.95	-0.07	1833.03	978212.22

PUBLISHED IN IJOG

The Free Air Anomaly (FAA) (Figure 4) was obtained by removing the elevation effect from the observed gravity. After correction, gravity values become more uniform, and the influence of topography is substantially reduced. The FAA map begins to highlight long-wavelength trends that correspond to deeper density variations. However, residual topographic effects and near-surface mass contributions are still present.

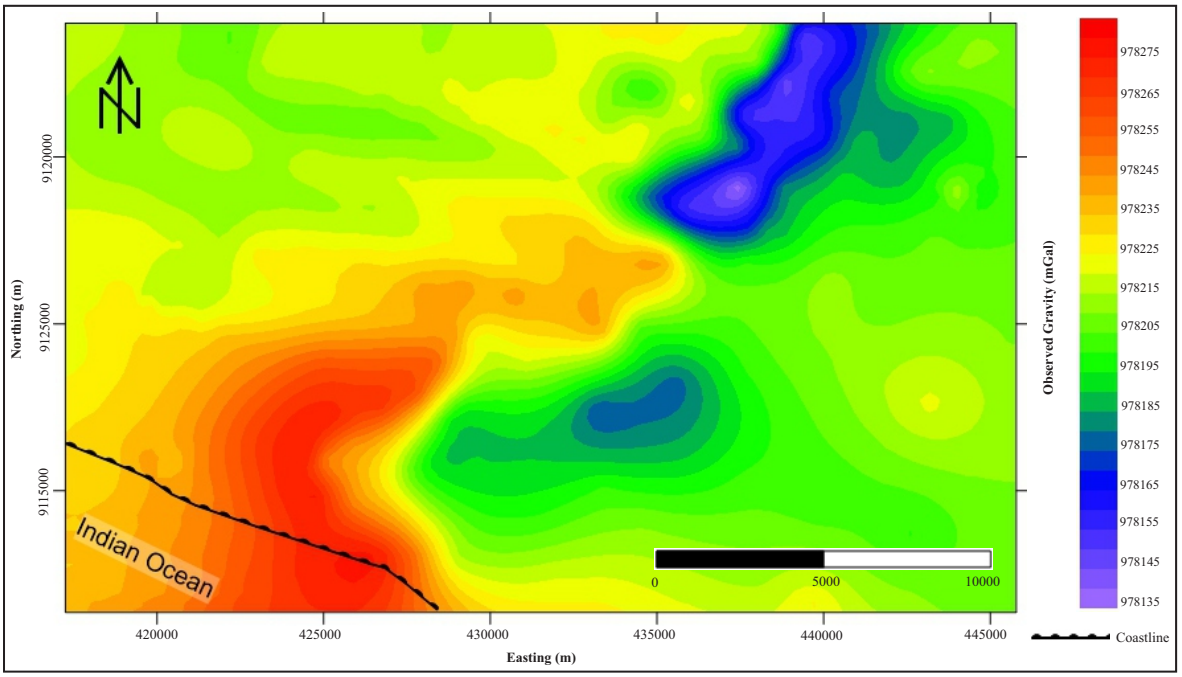


Figure 3. Observed gravity contour map obtained after tidal and drift corrections. The pattern is still strongly influenced by topography.

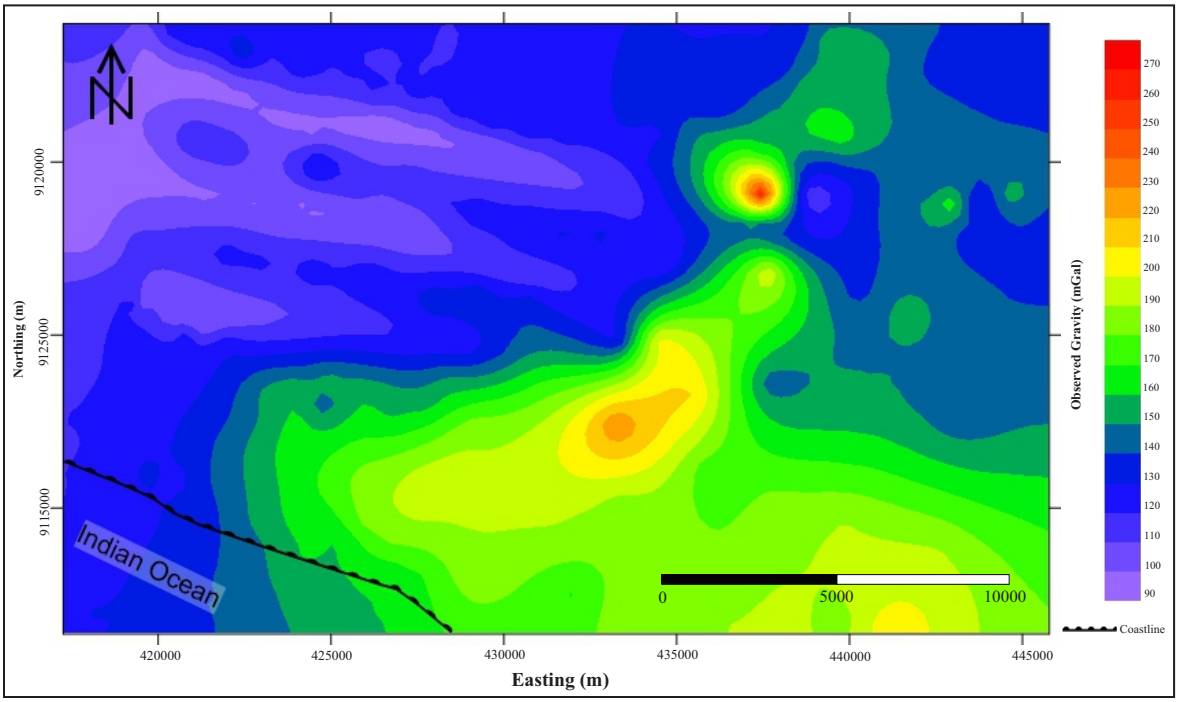


Figure 4. FAA contour map generated after applying free air correction to the observed gravity data.

PUBLISHED IN IJOG

The Simple Bouguer Anomaly (SBA) (Figure 5) incorporates a slab correction using an average rock density of 2.2 g/cm³. This correction further eliminates mass effects associated with surface topography. In the SBA map, the gravity field begins to reveal more distinct lateral density contrasts related to major geological units. High anomalies appear over the older volcano, whereas low anomalies align with younger volcanic deposits.

Complete Bouguer Anomaly

The Complete Bouguer Anomaly (CBA) map obtained from a series of data reductions is presented in Figure 6. The CBA values range from 70 to 310 mgal, with the lowest anomalies represented by purple to blue colours, while the highest anomalies are shown in yellow to red.

Residual and Regional Anomaly

The CBA represents a combination of gravity anomalies originating from both deep (low-frequency) and shallow (high-frequency) density sources. The desired anomalies in this study are the high-frequency components, referred to as residual gravity anomalies (Kebede *et al.*, 2020). Residual anomalies are obtained by separating the CBA from the low-frequency (regional) anomalies using the upward continuation method (Lucero *et al.*, 2025; Bahia *et al.*, 2025; Wuletawu *et al.*, 2024).

Figure 7 shows the regional gravity anomaly pattern, which exhibits a southeast-northwest contour trend represented by red to blue colours, with values ranging from 80 to 200 mGal. Figure 8 illustrates the residual gravity anomaly pattern, which is associated with shallow geological structures and has values ranging from -60 to 100 mGal. Figure 9 presents the results of the Euler deconvolution analysis, which provides an overview of the position and depth of the gravity anomaly sources.

2D Modelling

Gravity data modeling was carried out to obtain subsurface information based on rock density variations. The modeling process was performed through inversion with the objective of constructing a geological structural model related to the 2006 Yogyakarta earthquake. The inversion was conducted iteratively, updating the density contrast model until an optimal fit with the residual gravity data was achieved while minimizing the misfit value. A total of six 2D profiles were generated along northwest-southeast

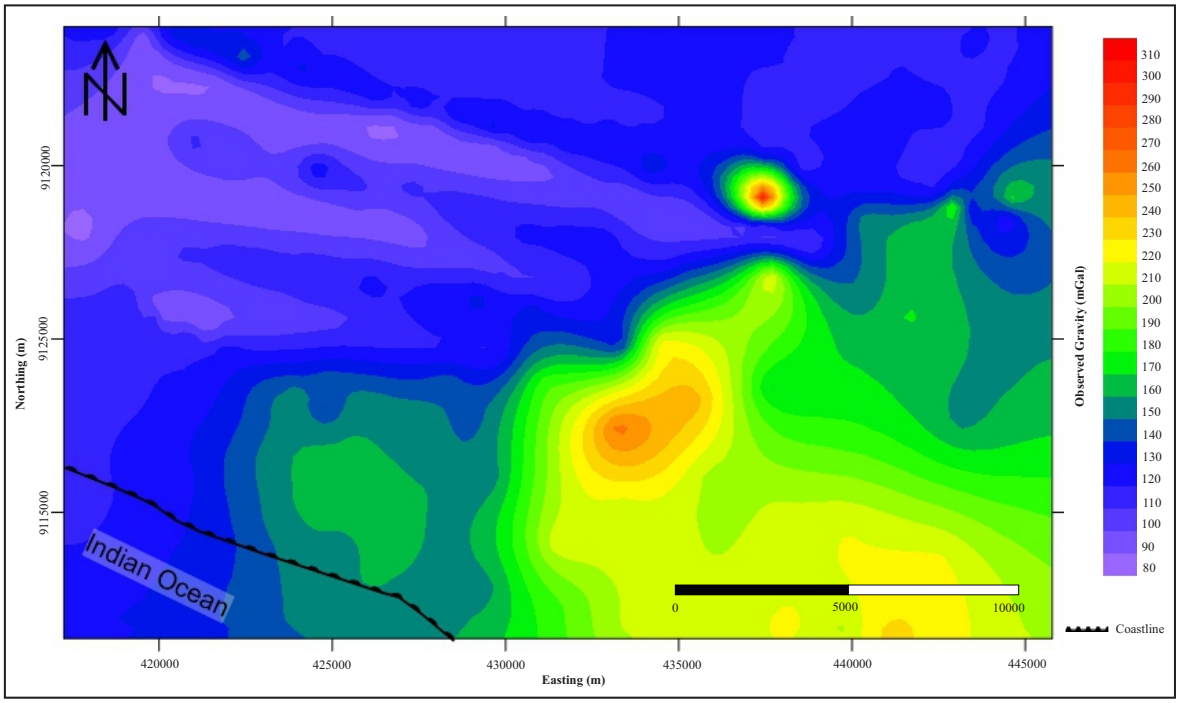


Figure 5. SBA contour map showing the distribution of subsurface density contrasts across the studied area.

PUBLISHED IN IJOG

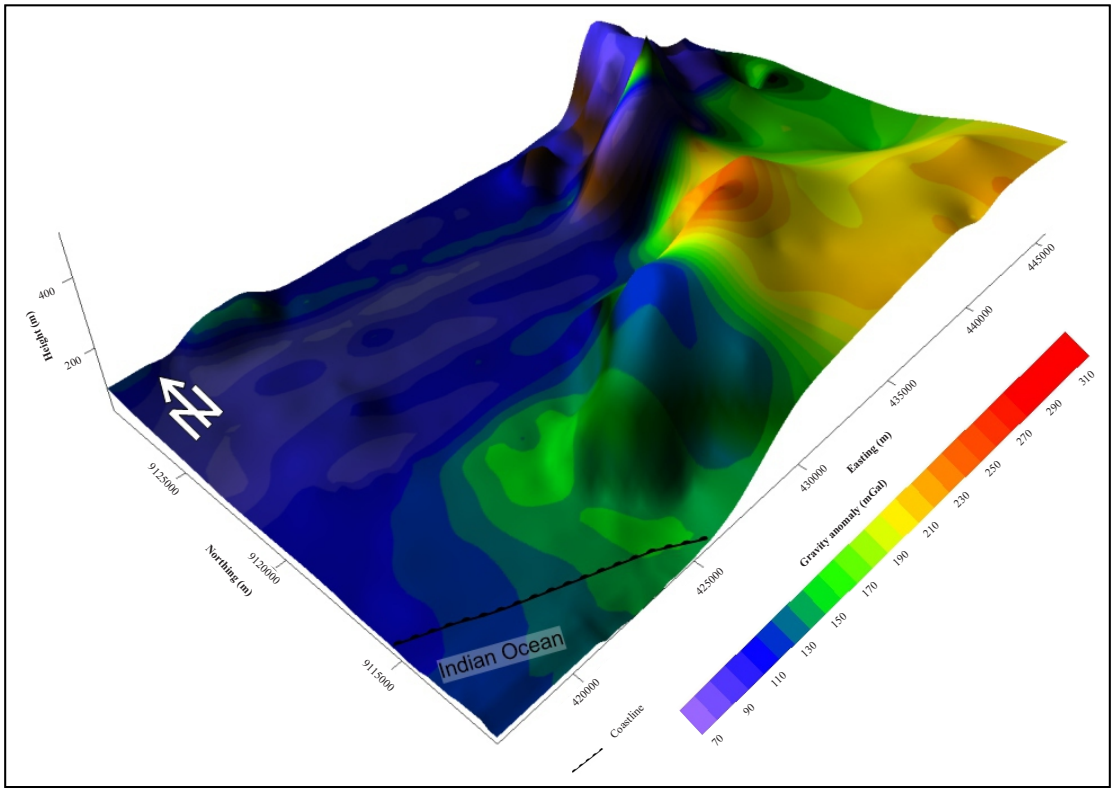


Figure 6. Three-dimensional topographic map overlaid with Complete Bouguer Anomaly (CBA) data of the studied area. The colour scale represents gravity anomaly values ranging from 70 to 310 mgal. where purple to blue indicates low anomalies and yellow to red indicates high anomalies.

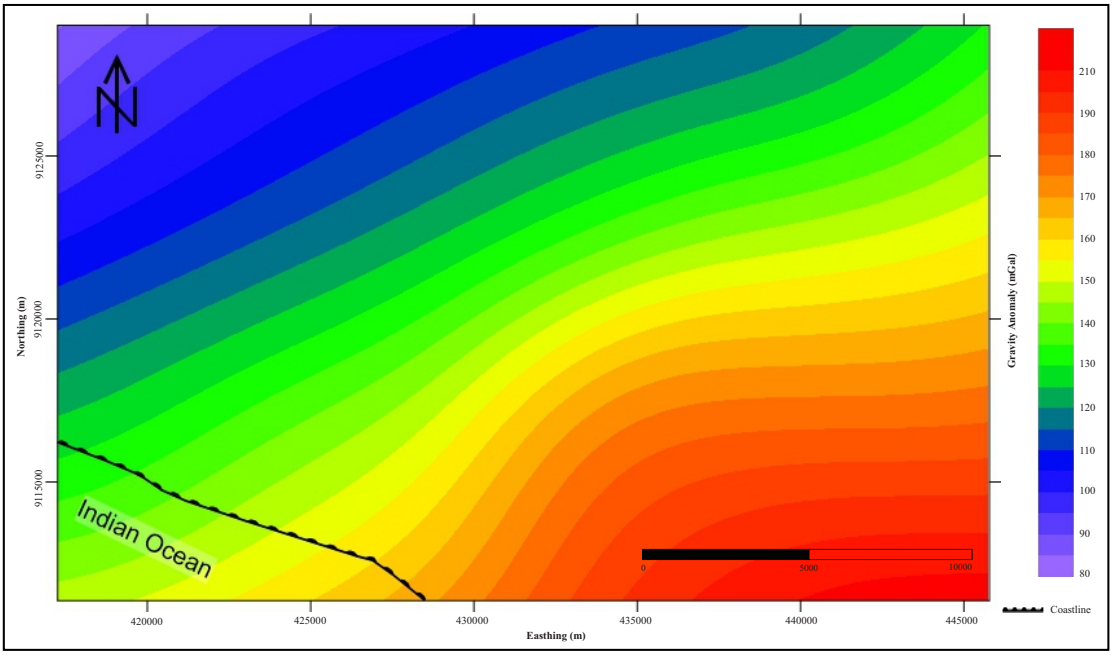


Figure 7. Regional anomaly, showing the broad and long-wavelength gravity trend.

directions, starting from Line L1 in the north to Line L6 in the south. These profiles cross the Opak Fault and the Ngalang Fault, with Line L3 specifically intersecting the mainshock zone of

PUBLISHED IN IJOG

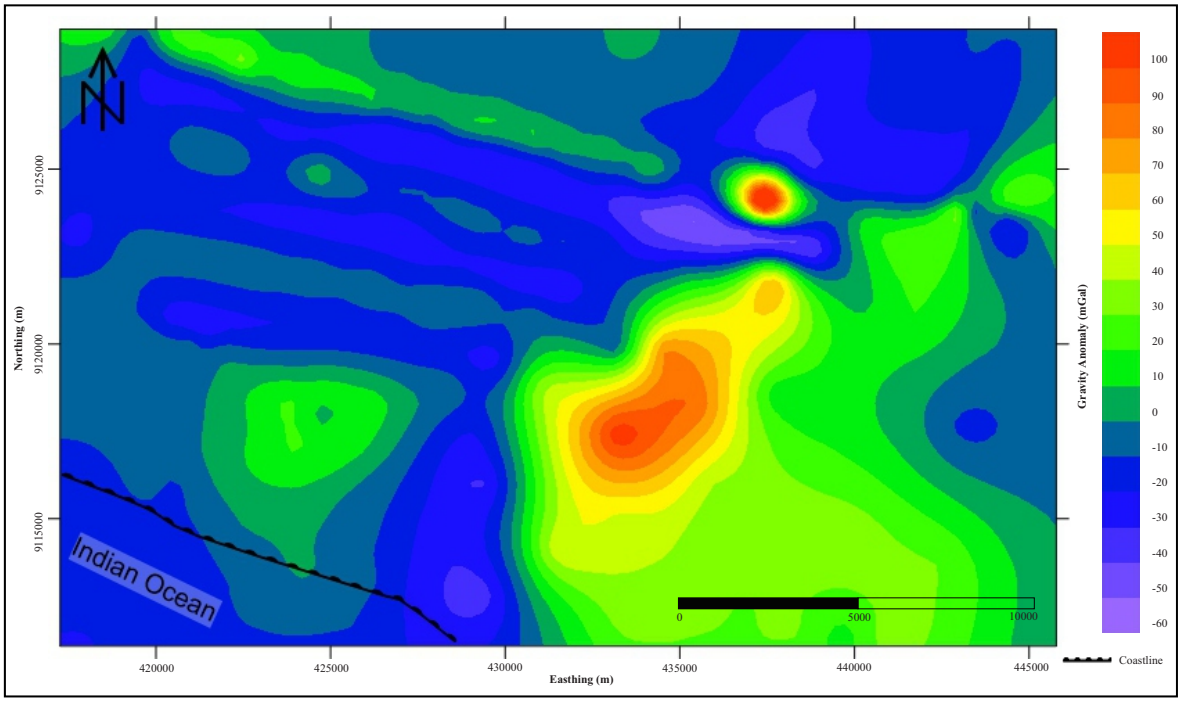


Figure 8. Residual anomaly, highlighting local and short-wavelength variations that are associated with shallow geological structures.

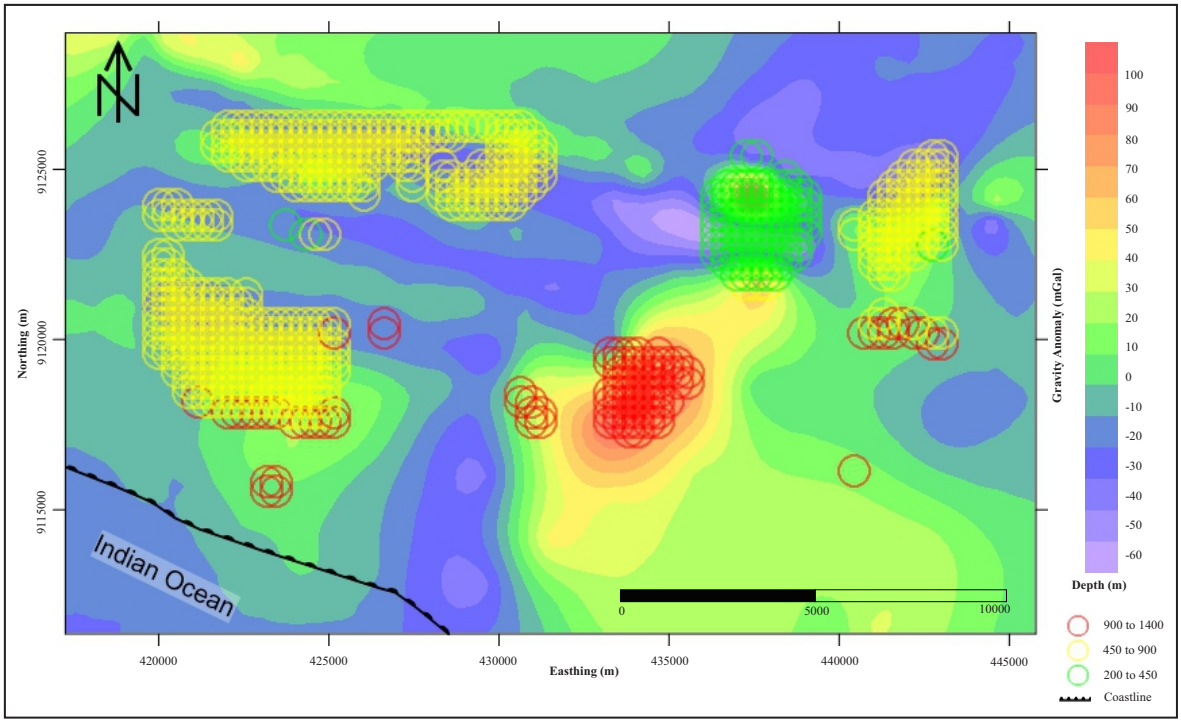


Figure 9. Gravity anomaly map of the studied area with Euler deconvolution solutions. The colour contour represents the gravity anomaly values (mgal), while the circles indicate estimated source depths: 200–450 m (green), 450-900 m (orange), and 900-1400 m (red).

the 2006 Yogyakarta earthquake. The modeled profiles are shown in Figure 10.

Figure 11 presents the 2D model showing density contrasts ranging from -0.5 g/cm³ to

PUBLISHED IN IJOG

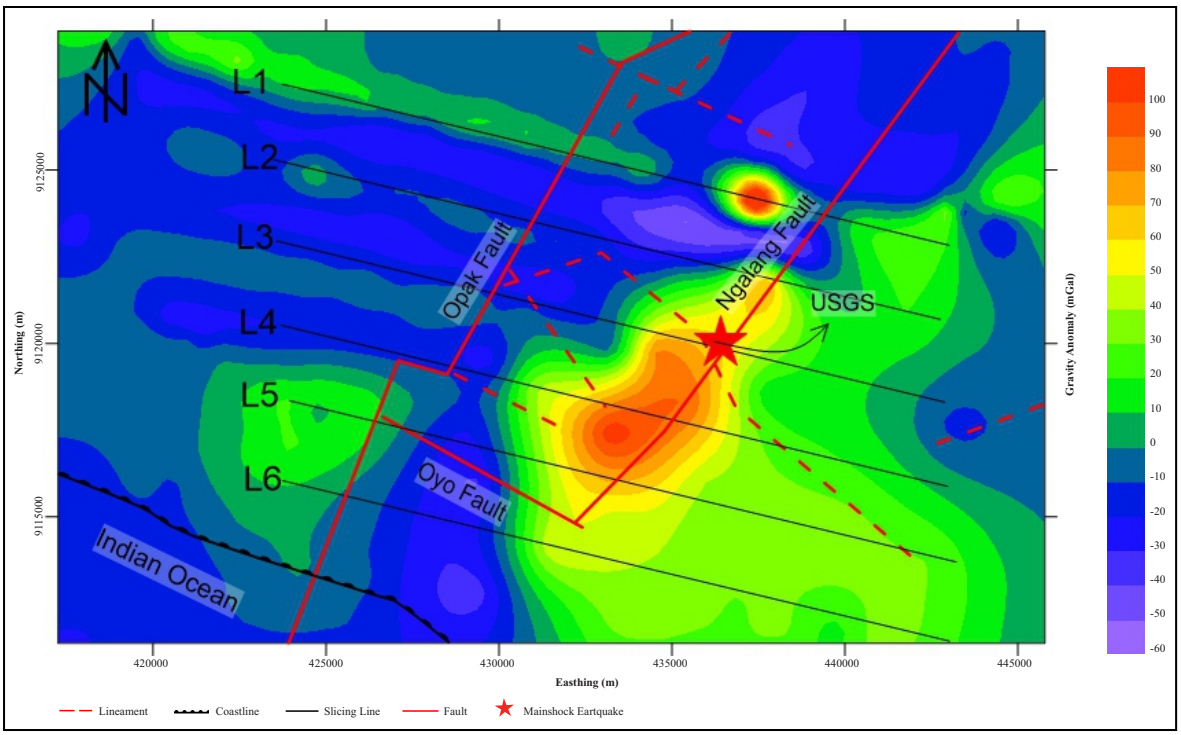


Figure 10. Residual gravity anomaly map of the studied area, showing the distribution of gravity anomaly values (mGal). The thick red lines mark the major faults (Opak, Nglanggeran, and Oyo Faults), and dashed red lines indicate lineaments. and black boxes with profiles (L1–L6) represent the cross-sections used for further analysis. The red star denotes the epicentre of the mainshock earthquake based on USGS data.

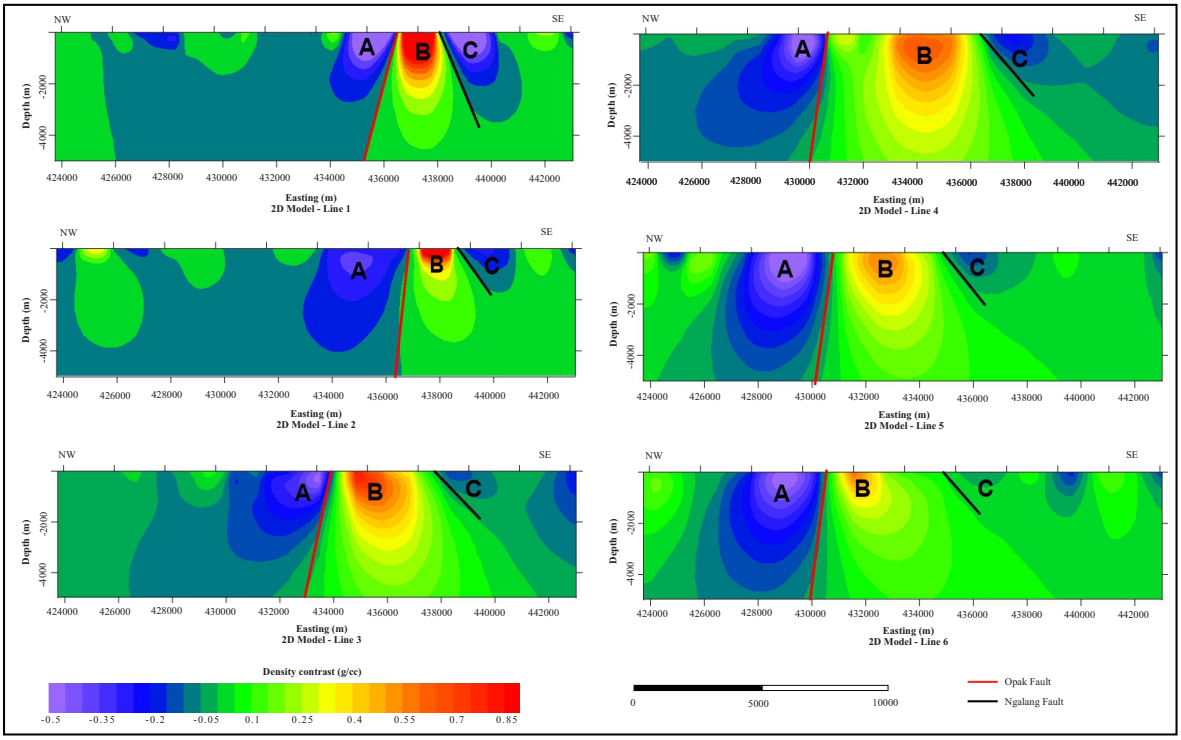


Figure 11. 2D inversion models of gravity data along six profiles (L1–L6) showing density contrast distribution (g/cm^3). The colour scale represents density contrast values ranging from –0.5 g/cm^3 (blue to purple, low density) to 0.85 g/cm^3 (yellow to red, high density). Labels A, B, and C indicate the main density anomaly zones interpreted along each profile. The solid red lines represent the Opak Fault, while the solid black lines denote the Ngalang Fault.

PUBLISHED IN IJOG

0.85 g/cm^3 relative to the average density of 2.2 g/cm^3. The density contrasts are grouped into three categories: density contrast A (low density on the western side of the Opak Fault), density contrast B (high density), and density contrast C (low density on the eastern side of the Ngalang Fault).

Density contrast A, with a range of -0.5 to -0.05 g/cm^3, was observed across all six profiles (L1-L6). Density contrast B, ranging from 0.4 to 0.85 g/cm^3, also appears in all six profiles (L1-L6), indicating the presence of the Nglanggeran Formation, which consists of older volcanic rocks such as andesite, lava, and breccia. Meanwhile, density contrast C, representing the low-density zone on the eastern side of the Nglanggeran Fault, is identified in profiles L1-L4, but gradually weakens and eventually disappears in L5 and L6.

Discussion

The distribution of high Bouguer anomalies (Figure 2) was observed in the Wonosari Formation highlands, reflecting the dominance of Miocene carbonate rocks with relatively high density. This condition arises, because carbonate rocks that have undergone diagenesis are generally more compact and denser, thus producing a positive gravity response. Conversely, the low anomalies recorded in the northern part indicate the presence of Quaternary volcanic deposits and the Sentolo Formation. These lithologies, which consist of sandstones, clays, and marls, have lower densities compared to carbonates. Such differences may represent both structural controls and sedimentary processes that infilled the basin, as also explained by Widijono and Setyanta (2007) and Pohan *et al*. (2023). Therefore, the distribution of Bouguer anomalies can be utilized to infer lithological contrasts and to understand the tectonic evolution of the southern Yogyakarta region.

The regional anomaly values ranging between 170-200 mgal (Figure 7) reflect the existence of older, denser rocks at greater depths. This condition indicates the presence of basement rocks or more compact geological structures beneath the studied area. In contrast, the low anomalies (80-140 mgal), represented by green to blue colours, are more closely related to younger sediments and volcanic deposits. A transitional yellow zone separating the two anomaly patterns highlights contrasting rock properties and is strongly associated with The Opak Fault as the principal structure controlling density contrasts in the area (Permana *et al*., 2024).

At shallower scales, the residual anomalies provide a more detailed representation of the near-surface to intermediate geological conditions (Figure 8). High anomalies (40-100 mgal) in the Imogiri and Mangunan areas correlate with Miocene carbonate rocks of The Wonosari Formation as well as volcanic rocks from the Semilir, Nglanggeran, and Sambipitu Formations (Atmoko *et al*., 2018; Ansori *et al*., 2022). In contrast, low anomalies (-60 to 40 mGal) dominate the Bantul Basin, which is filled by young volcanic deposits of Mount Merapi. These low anomalies also display a north-south trend, interpreted as the trace of the Opak Fault, an active structure that controls basin development (Maghfira *et al*., 2022; Azifah *et al*., 2025).

The Euler deconvolution results (Figure 9) reveal the distribution of gravity anomaly source depths forming linear patterns that can be interpreted as fault zones marking the boundaries between rock formations, such as the transition between the Sentolo and Wonosari Formations. Depth solutions ranging between 900-1400 m are associated with high Bouguer anomalies (40-100 mgal), indicating a direct correlation with active faults, particularly the Opak Fault to the west and the Ngalang Fault to the east. This condition suggests the presence of a fault-bounded uplift zone formed by tectonic activity, underscoring the critical role of faults in controlling subsurface structure, morphology, and seismic potential in the studied area.

The distribution of density groups obtained from the inversion further highlights the relationship between lithology, geological structures, and seismic potential. Density group A (-0.5 to -0.05 g/cm^3), consistently present in all profiles

PUBLISHED IN IJOG

(L1-L6), is associated with the Semilir Formation, which consists of tuff and undifferentiated volcanic rocks. Density group B (0.4 to 0.85 g/cm^3), also found across all profiles, is interpreted as the Nglanggeran Formation, composed of older volcanic rocks such as lava, andesite, and breccia. Interestingly, density group C (low density) dominates only the northern sections (L1-L4), but weakens and disappears in the southern profiles (L5-L6) due to the lithological homogeneity of the Wonosari Formation.

The presence of low-density zones in L1-L4 (Figure 11) suggests a more complex geological composition, involving the Wonosari and Sambipitu Formations. Spatially, the three density groups (A, B, and C) exhibit a westward shift, following the tectonic trend influenced by the Opak Fault, which becomes more westward toward the south. The Opak Fault acts as a boundary between older rock units and younger Merapi volcanic products, whereas the Ngalang Fault functions as a cross-cutting structure that truncates the Semilir, Nglanggeran, and Sambipitu Formations (Saputra *et al*., 2018; Sutiono *et al*., 2022). These results are consistent with the 2D models (Figure 11), which support the findings of Ramdhan (2025) and USGS observations that the mainshock of the 2006 Yogyakarta earthquake originated from the Ngalang Fault. Thus, the identification of low-density rocks (Group C, -0.5 to -0.05 g/cm^3) plays a significant role as the seismogenic unit, confirming the close relationship between density distribution, active faults, and seismic potential in the studied area.

Furthermore, several microtremor studies conducted in the same region provide consistent evidence supporting the gravity-based interpretation. Microtremor analyses along the Opak Fault in Bantul and Imogiri indicate high seismic vulnerability (Kg) and low dominant frequencies in Quaternary sedimentary zones, implying thick unconsolidated deposits (Marsyelina *et al*., 2014; Putra *et al*., 2022). Similarly, Wibowo *et al*. (2023) reported that areas underlain by alluvial and volcanic deposits near the Opak River exhibited significant site amplification effects, which corresponded spatially with the low-density zones identified in this study. The agreement between gravity and microtremor results reinforces the interpretation that the Opak Fault and adjacent sedimentary basins play a major role in controlling seismic amplification and energy propagation during earthquakes in southern Yogyakarta.

Conclusions

The use of gravity field data combined with a series of reductions and 2D inversion modeling provides significant insights into the geological structures of southern Yogyakarta. The 2D inversion results successfully outlined the Opak and Ngalang Faults, which control structural configuration and seismic potential of the area. The 2D inversion results also reveal that the earthquake source region correlates with a low-density contrast (-0.5 to -0.05 g/cm^3 relative to the average density of 2.2 g/cm^3), which indicates the presence of weak materials that are more susceptible to deformation. Furthermore, the inversion also delineates areas with high-density contrasts (0.4-0.85 g/cm^3 relative to the average density of 2.2 g/cm^3), which are interpreted as older volcanic rocks such as lava, andesite, and breccia from The Nglanggeran Formation.

The main strength of this study lies in the gravity inversion and structural interpretation, which provide valuable insight into subsurface conditions in an active fault zone. Nevertheless, some limitations remain due to the spatial resolution of gravity data and the absence of direct subsurface validation, which may affect the accuracy of fault geometry estimation. Further research should integrate gravity data with other geophysical methods such as microtremor, magnetotelluric, or seismic surveys to improve model constraints and interpretation reliability. High-resolution gravity measurements are also recommended for more detailed mapping of fault structures. Overall, the findings of this study may serve as a scientific basis for spatial planning, the determination of evacuation routes, and the development of

PUBLISHED IN IJOG

earthquake-resistant infrastructure in vulnerable regions, particularly around active fault zones.

Acknowledgements

The authors would like to express their sincere gratitude to the Geophysics Laboratory, Universitas Gadjah Mada (UGM), for providing the gravimeter, GPS instruments, and technical support during the data acquisition process.

References

Ansori, A., Setiawam, N.I., Warmada, I.W., and Yogaswara, H., 2022. Identification of Geodiversity and Evaluation of Geosites to Determine Geopark Themes of Karangsambung-Karangbolong National Geopark, Kebumen, Indonesia. *International Journal of Geoheritage and Parks,* 10 (1), p.1-15. DOI: 10.1016/j.ijgeop.2022.01.001

Atmoko, D.D., Titisari, A.D., and Idrus, A., 2018. Geochemical characteristics of limestone of Wonosari-Punung Formation, Gunungkidul Regency, Yogyakarta, Indonesia. *Indonesian Journal on Geoscience*, 5 (2), p.179-197. DOI: 10.17014/ijog.5.2.179-197

Azifah, G.B., Fathani, T.F., and Setiawan, H., 2025. Seismic microzonation studies in the Southern part of Progo River, Special Region of Yogyakarta, Indonesia. *Geoenvironmental Disasters*, 12 (1), p.1-33. DOI: 10.21203/rs.3.rs-4939527/v1

Bahia, M.E., Benedini, L., Gregori, D.A., and Gómez, J.I., 2025. Understanding the fracture-volcanism pattern: Gravity and magnetic characterization of the Early Jurassic pull-apart structure in the Western Northpatagonian Region, Argentina. *Journal of South American Earth Sciences*, 151, p.105259. DOI: 10.1016/j.jsames.2024.105259

Blakely, R.J., 1996. *Potential theory in gravity and magnetic applications*. Cambridge: Cambridge University Press.

Diambama, A.D., Anggraini, A., Nukman, M., Lühr, B.G., and Suryanto, W., 2019. Velocity structure of the earthquake zone of the M6.3 Yogyakarta earthquake 2006 from a seismic tomography study. *Geophysical Journal International*, 216 (1), p.439-452. DOI: 10.1093/gji/ggy430

Famiani, D., Brunori, C.A., Pizzimenti, L., Cara, F., Caciagli, M., Melelli, L,. and Barchi, M.R., 2020. Geophysical reconstruction of buried geological features and site effects estimation of the Middle Valle Umbra basin (Central Italy). *Engineering Geology*, 269, p.105543. DOI: 10.1016/j.enggeo.2020.105543

Fitrianingtyas, R., Al Hakim, M.F., Wibowo, A., and Aziz, K.N., 2023. Seismicity analysis in Yogyakarta based on hypocentre relocation using double-difference method. *Jurnal Sains Dasar*, 12 (1), p.62-70. DOI: 10.21831/jsd.v12i1.60118

Handayani, L., 2019. Active fault zones of the 2006 Yogyakarta earthquake inferred from tilt derivative analysis of gravity anomalies. *Geology and Mining Research*, 29 (1), p.1-11. DOI: 10.14203/risetgeotam2019.v29.1018

Handayani, L., Mukti, M.M., Arisbaya, I., Gaol, K.L., Sudrajat, Y., Lubis, A.M., and Anggono, T., 2025. Basement structure across Renun segment near Toba caldera inferred from the gravity anomaly: Implication for potential earthquake rupture barrier. *Geodesy and Geodynamics*. 17 (1), p.35-44. DOI: 10.1016/j.geog.2025.04.006

Hasanudin, Z.A., Andreas, H., Meilano, I., Gamal, M., Gumilar, I., and Abdullah, C.I., 2009. Deformasi koseismik dan pascaseismik gempa Yogyakarta 2006 dari hasil survei GPS. *Indonesian Journal on Geoscience,* 4 (4), p.275-284. DOI: 10.17014/ijog.4.4.275-284

Kebede, H., Alemu, A., and Fisseha, S., 2020. Upward continuation and polynomial trend analysis as a gravity data decomposition: Case study at Ziway-Shala Basin, Central Main Ethiopian Rift. *Heliyon*, 6 (1), p.1-11. DOI: 10.1016/j.heliyon.2020.e03292

PUBLISHED IN IJOG

Librian, V., Ramdhan, M., Nugraha, A.D., Mukti, M.M., Syuhada, S., Lühr, B.G., and Husni, Y.M.R., 2024. Detailed seismic structure beneath the earthquake zone of Yogyakarta 2006 (Mw~6.4), Indonesia, from local earthquake tomography. *Physics of the Earth and Planetary Interiors*, 351, p.107170. DOI: 10.1016/j.pepi.2024.107170

Lucero, S.V., Almaraz, F., Prezzi, C.B., Ghidella, M., and Vizán, H., 2025. Tectonic structures of SW margin of Gondwana from gravity and magnetic anomalies of the Río de la Plata area and their correlation with the Beattie Magnetic Anomaly in South Africa. *Tectonophysics,* 894, p.230571. DOI: 10.1016/j.tecto.2024.230571

Maghfira, P.D., Utami, P., and Niasari, S.W., 2022. Heat flow and gravity anomalies in some presumed hidden geothermal prospects in Java. *IOP Conference Series: Earth and Environmental Science*, 1071 (1), p.012025. DOI: 10.1088/1755-1315/1071/1/012025

Mahendra, K.O., Zakariah, M.N.A., Satiawan, S., Suwardi, B.N., and Widjanarko, E., 2026. Full Tensor Gravity GradiometrySensitivity Analysis for Delineating Lateral Reservoir Boundaries and Subtle Density Contrasts. *Scientific Contributions Oil and Gas*, 49 (3) p.67-87. DOI: 10.29017/scog.v49i3.2116

Marsyelina, M., Wibowo, N. B., and Darmawan, D. 2014. Microtremor Characteristics and Analysis of Seismicity on Opak Fault Lines, Bantul District, Yogyakarta. *Jurnal Sains Dasar,* 2 (1), p.95-101.

Moon, S.W., Hashash, Y.M., and Park, D., 2017. USGS hazard map compatible depth-dependent seismic site coefficients for the Upper Mississippi Embayment. *KSCE Journal of Civil Engineering,* 21 (1), p.220-231. DOI: 10.1007/s12205-016-0681-4

Mulyaningsih, S., 2021. Earthquakes, volcanic eruptions, and other geological disasters during historical records in Yogyakarta Special Region, Indonesia. *Indonesian Journal on Geoscience*, 8 (2), p.197-212. DOI: 10.17014/ijog.8.2.197-212

Nowell, D.A.G., 1999. Gravity terrain corrections-an overview. *Journal of Applied Geophysics*, 42 (2), p.117-134. DOI: 10.1016/S0926-9851(99)00028-2

Panzera, F., Tortorici, G., Romagnoli, G., Marletta, G., and Catalano, S., 2020. Empirical evidence of orthogonal relationship between directional site effects and fracture azimuths in an active fault zone: The case of the Mt. Etna lower eastern flank. *Engineering Geology*, 279, p.105900. DOI: 10.1016/j.enggeo.2020.105900

Perdana, A.R.A. and Castello, J.V., 2025. Shattered ground, shaken minds: Mental health consequences of earthquakes. *Economics & Human Biology*, 56, p.101448. DOI: 10.1016/j.ehb.2024.101448

Permana, N.R., Fadrian, D.F., Gunawan, B., and Wulandari, A., 2024. Distribution of geological structures on Java Island based on derivative analysis of satellite gravity data. *Jurnal Penelitian Fisika dan Aplikasinya (JPFA)*, 14 (2), p.154-168. DOI: 10.26740/jpfa.v14n2.p154-168

Pohan, A.F., Sismanto, S., Nurcahya, B.E., Lewerissa, R., Koesuma, S., Saputro, S.P., and Adhi, M.A., 2023. Utilization and modeling of satellite gravity data for geohazard assessment in the Yogyakarta area of Java Island, Indonesia. *Kuwait Journal of Science*, 50 (4), p.499-511. DOI: 10.1016/j.kjs.2023.05.016

Putra, M.F.N., Rustadi., Haerudin, N., and Sulaeman, C., 2022. Analisis Site Effect Berdasarkan Data Mikrotremor dan Nilai Peak Ground Acceleration pada Sesar Opak, Kabupaten Bantul Daerah Istimewa Yogyakarta. *Jurnal Geofisika Eksplorasi,* 3 (3).

Ramdhan, M., Priyobudi, P., Mukti, M.M., Putra, A.S., Hidayat, E., Muttaqy, F., and Wandono, W., 2025. Tracing fault systems from subsurface to surface in Yogyakarta and its surroundings, Indonesia. *Natural Hazards Research*, 6, p.237-250. DOI: 10.1016/j.nhres.2025.07.003

Rizkianto, Y., Nugroho, M.O., Rachman, M.G., Pratama, J., and Marpaung, A.T.M., 2022. Paleobatimetri satuan batupasir karbonatan

PUBLISHED IN IJOG

Formasi Sambipitu di lintasan Kali Ngalang, Gedangsari, Gunungkidul, Yogyakarta. *Jurnal Geologi*, 5 (1), p.42-52. DOI: 10.14710/jgt.5.1.2022.42-52

Saputra, A., Gomez, C., Delikostidis, I., Zawar-Reza, P., Hadmoko, D.S., Sartohadi, J., and Setiawan, M.A., 2018. Determining earthquake susceptible areas southeast of Yogyakarta, Indonesia-Outcrop analysis from structure-from-motion (SfM) and geographic information system (GIS). *Geosciences,* 8 (4), p.132. DOI: 10.3390/geosciences8040132

Surono, 2008. Sedimentasi Formasi Semilir di Desa Sendang Wuryanto, Wonogiri, Jawa Tengah. *Geo-dynamics*, 18 (1), p.29-41. DOI: 10.33332/jgsm.geologi.v18i1.225

Sutiono, A., Prastistho, B., Prasetyadi, C.P.C., and Supartoyo, S., 2022. Opak Fault strand delineation using Merapi slope shifted indicator. *Journal of Applied Geology*, 7 (1), p.35-40. DOI: 10.22146/jag.55276

Telford, W.M., Geldart, L.P., and Sheriff, R.E., 1990. *Applied geophysics*. Cambridge: Cambridge University Press.

Tsuji, T., Yamamoto, K., Matsuoka, T., Yamada, Y., Onishi, K., Bahar, A., and Abidin, H.Z., 2009. Earthquake fault of the 26 May 2006 Yogyakarta earthquake observed by SAR interferometry. *Earth, Planets and Space*, 61 (7), p.e29-e32. DOI: 10.1186/BF03353189

Walter, T.R., Wang, R., Luehr, B.G., Wassermann, J., Behr, Y., Parolai, S., and Zschau, J., 2008. The 26 May 2006 magnitude 6.4 Yogyakarta earthquake south of Mt. Merapi volcano: Did lahar deposits amplify ground shaking and thus lead to the disaster? *Geochemistry, Geophysics, Geosystems,* 9 (5), p.1-9. DOI: 10.1029/2007GC001810

Wibowo, N. B., Fathani, T. F., Pramumijoyo, S., and Marliyani, G.I., 2023. Microzonation of Seismic Parameters in Geological Formation Units Along the Opak River using Microtremor Measurements. *International Journal of Geomate,* 25 (110), p.208-219. DOI: 10.21660/2023.110.4017

Widijono, B.S. and Setyanta, B., 2007. Anomali gaya berat, kegempaan, serta kelurusan struktur geologi daerah Jogjakarta dan sekitarnya. *Jurnal Geologi dan Sumberdaya Mineral*, 17 (2), p.74-90. DOI: 10.33332/jgsm.geologi.v17i2.281

Wuletawu, H., Alemu, A., Nigussie, W., Mickus, K., Keir, D., Wendwesen, S., and Wassihun, S., 2024. The subsurface anatomy of a mid-upper crustal magmatic intrusion zone beneath the Boku volcanic complex, Main Ethiopian Rift inferred from gravity data. *Journal of Volcanology and Geothermal Research*, 452, p.108133. DOI: 10.1016/j.jvolgeores.2024.108133

Yilmaz, N., 2023. Gravity data reduction, Bouguer anomaly, and gravity disturbance. *Geofizicheskiy Zhurnal*, 45 (6). DOI: 10.24028/gj.v45i6.293314

PUBLISHED IN IJOG